NAVY DEPARTMENT
THE DAVID W. TAYLOR MODEL BASIN
WASHINGTON 7, D.C.

AN ELECTROLYTIC TANK DEVELOPED FOR OBTAINING VELOCITY AND PRESSURE DISTRIBUTIONS ABOUT HYDRODYNAMIC FORMS

by

A. Borden, G.L. Shelton, Jr., and W.E. Ball, Jr.

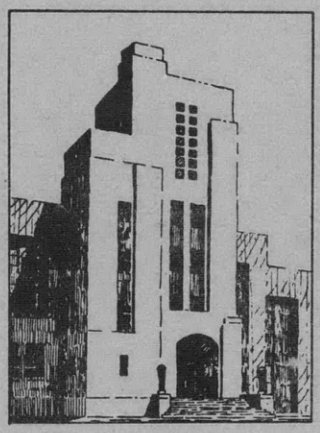

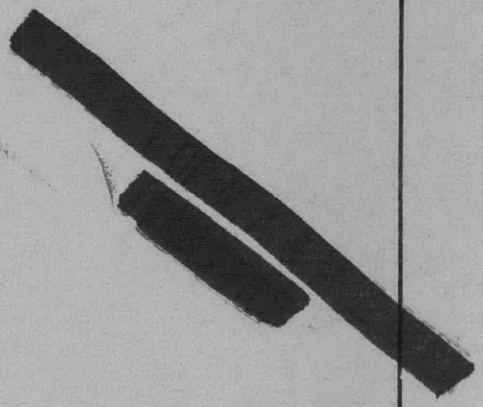

April 1953

Report 824

AN ELECTROLYTIC TANK DEVELOPED FOR OBTAINING VELOCITY AND PRESSURE DISTRIBUTIONS ABOUT HYDRODYNAMIC FORMS

by

A. Borden, G.L. Shelton, Jr., and W.E. Ball, Jr.

April 1953 Report 824

TABLE OF CONTENTS

NOTATION

E	Electric field intensity
h	Depth of medium
i_x	x component of electric current
i_y	y component of electric current
i_z	z component of electric current
p	Pressure
s	Arc length
U_0	Free-stream velocity
V	Electric potential function
v_t	Tangential velocity
v_x	x component of velocity
v_y	y component of velocity
v_z	z component of velocity
w	Complex velocity potential function
x	Longitudinal direction
y	Transverse direction
z	Vertical direction
ρ	Mass density of fluid
σ	Specific resistance of medium
ϕ	Hydrodynamic potential function
ψ	Hydrodynamic stream function

ABSTRACT

The design and development of an electrolytic tank is described and a discussion is given of some of the difficulties encountered in putting the tank into operation. The techniques developed for finding the velocity and pressure distributions about cylindrical bodies and about three-dimensional bodies of revolution are described, and some results obtained for bodies with known velocity and pressure distributions are presented.

INTRODUCTION

An electrolytic tank has been constructed and put into operation at the David Taylor Model Basin as part of a project to study the hydrodynamic flow about torpedoes and other bodies.[1] In this tank it is possible to survey velocity distributions of the potential flow about two-dimensional bodies and three-dimensional bodies of revolution with an accuracy comparable to that obtained by direct measurement in the towing basin or water tunnel. The method may eventually be extended to study more general types of flow on three-dimensional bodies, pressure distributions on a ship model, pressure distributions induced on a nearby wall by a moving body, etc.

Electrolytic tanks have been built at many laboratories both in this country and abroad. Two-dimensional tanks were built at the National Physical Laboratory in England before 1930,[2,3] and during the next twenty years L. Malavard and his colleagues perfected techniques and extended applications to many problems of aerodynamics.[4-7] The method has also been extended to determine the flow about three-dimensional bodies, particularly to bodies of revolution, flow through conduits, etc.

This paper describes the electrolytic tank which has been built at the Taylor Model Basin for two- and three-dimensional studies, reports the techniques developed for obtaining pressure distributions, and discusses the difficulties which have been encountered.

THEORETICAL CONSIDERATIONS

The steady irrotational flow of an incompressible inviscid fluid may be represented by a potential function $\phi\,(x, y, z)$ which is a solution of the Laplace equation (see standard texts in hydrodynamics, e.g., Lamb.[8])

$$\Delta\phi = \frac{\partial^2\phi}{\partial x^2} + \frac{\partial^2\phi}{\partial y^2} + \frac{\partial^2\phi}{\partial z^2} = 0 \qquad [1]$$

---

[1] References are listed on page 28.

Lines of constant ϕ, known as the velocity potential, are everywhere normal to the direction of flow, and the velocity components are obtained from the gradient of this function.

$$v_x = \frac{\partial \phi}{\partial x} \qquad v_y = \frac{\partial \phi}{\partial y} \qquad v_z = \frac{\partial \phi}{\partial z} \qquad [2]$$

Equations [1] and [2] are valid for both two- and three-dimensional flows.

The Laplace equation with similar boundary conditions also occurs in other fields of physics, particularly in electrostatics where the electric potential V satisfies the Laplace equation

$$\Delta V = \frac{\partial^2 V}{\partial x^2} + \frac{\partial^2 V}{\partial y^2} + \frac{\partial^2 V}{\partial z^2} = 0 \qquad [3]$$

The components of electric current are obtained from the gradient of V:

$$i_x = \frac{h}{\sigma}\frac{\partial V}{\partial x} \qquad i_y = \frac{h}{\sigma}\frac{\partial V}{\partial y} \qquad i_z = \frac{h}{\sigma}\frac{\partial V}{\partial z} \qquad [4]$$

where σ is the specific resistance of the medium and h the depth of the medium. Since the forms of the equations are identical, it is possible to determine the hydrodynamic flow from a study of the electrical counterpart in which the hydrodynamic velocity potential ϕ corresponds to the electric potential V. Such analogies are possible both in two- and three-dimensional flows whether the flow is axisymmetrical or not.

In two-dimensional flow and in three-dimensional flow in which there is an axis of symmetry, there exists a system of stream functions ψ which are constant along lines of flow and are everywhere orthogonal to equipotential lines. In two-dimensional flow, ψ as well as ϕ is a potential function and satisfies the Laplace equation. Hence, ϕ and ψ may be represented as the real and imaginary parts, respectively, of a complex potential function:

$$w(x, y) = \phi(x, y) + i\,\psi(x, y) \qquad [5]$$

The velocity components in terms of ϕ and ψ are given by the Cauchy-Riemann equations:

$$v_x = \frac{\partial \phi}{\partial x} = -\frac{\partial \psi}{\partial y}$$

$$v_y = \frac{\partial \phi}{\partial y} = \frac{\partial \psi}{\partial x} \qquad [6]$$

In the two-dimensional electric field analogy, a system of lines of constant electrical flux E exists which forms an orthogonal network with the lines of constant electrical potential, where E also satisfies the Laplace equation. Thus, V and E may also be represented as the real and imaginary parts of a complex potential function:

$$f(x, y) = V(x, y) + i\,E(x, y) \qquad [7]$$

The components of current are

$$i_x = \frac{h}{\sigma}\frac{\partial V}{\partial x} = -\frac{h}{\sigma}\frac{\partial E}{\partial y}$$

$$i_y = \frac{h}{\sigma}\frac{\partial V}{\partial y} = \frac{h}{\sigma}\frac{\partial E}{\partial x} \qquad [8]$$

Since the stream function and velocity potential satisfy identical equations for two-dimensional flow, the role of ϕ and ψ may be interchanged. Thus, in setting up an electrical analogy, the streamlines ψ may be represented either by V or E and the equipotential lines ϕ by the other function. Either one of two analogies may be used in an electrolytic tank.

$$\text{Analogy A:} \quad \phi \equiv V \quad \psi \equiv E \qquad [9]$$

A dielectric model representing the hydrodynamic body is placed in a semiconducting medium in such a way that equipotential lines correspond to lines of constant electric potential and streamlines correspond to lines of constant electric flux.

$$\text{Analogy B:} \quad \phi \equiv E \quad \psi \equiv V \qquad [10]$$

A conducting model representing the hydrodynamic body is placed in a dielectric medium in such a way that the equipotential lines of flow correspond to lines of constant electric flux and streamlines correspond to lines of constant electric potential.

When the flow is three-dimensional with axial symmetry, the physical interpretation of the stream function is somewhat different from that in two-dimensional flow. Since in three dimensions the stream functions define surfaces across which there is no flow, the stream function at any point in the medium is proportional to the flux of flow through a surface generated by the revolution about the symmetry axis of any curve joining this point with the axis. The velocity components parallel and normal to the symmetry axis are respectively:[8]

$$v_x = \frac{\partial \phi}{\partial x} = -\frac{1}{y}\frac{\partial \psi}{\partial y}$$

$$v_y = \frac{\partial \phi}{\partial y} = \frac{1}{y}\frac{\partial \psi}{\partial x} \qquad [11]$$

Since the stream function here is a measure of the flux of flow through a surface rather than the flow across a line in two-dimensional flow, the dimensions of ψ are no longer the same as those of ϕ and the form of the equations defining the velocity components [11] is different from that of [6]. Although ϕ still satisfies the Laplace equation, ψ does not. By use of the continuity equation and the condition of irrotationality of the motion, the differential equations

for ϕ and ψ are:

$$\frac{\partial^2 \phi}{\partial x^2} + \frac{\partial^2 \phi}{\partial y^2} + \frac{1}{y}\frac{\partial \phi}{\partial y} = 0$$

$$\frac{\partial^2 \psi}{\partial x^2} + \frac{\partial^2 \psi}{\partial y^2} - \frac{1}{y}\frac{\partial \psi}{\partial y} = 0 \qquad [12]$$

In the three-dimensional electrical analogue, equations analogous to [9] and [10] hold in V and E. Since E no longer satisfies the Laplace equation, E and V are also not interchangeable in the electrical analogy. Hence, Analogy A in which $\phi \equiv V$ and $\psi \equiv E$ is almost always used in electrolytic tank studies. If Analogy B is used, it is necessary to employ a sloping tank, in which the depth of electrolyte varies as $1/r$.

No stream function exists in three-dimensional flow in which there is no axis of symmetry. Analogy A may still be applied to this case, however, since there is still a complete correspondence between the hydrodynamic equipotential lines and the lines of constant electrical potential. The velocity components are still proportional to the gradient of the electric potential.

There are a number of ways in which the electrical analogies have been realized, and numerous papers have been written on special problems which have been solved with the aid of an electrolytic tank and other rheoelectric methods. It is not the purpose of this report to review all possible uses of an electrolytic tank but rather to describe the TMB electrolytic tank and the techniques developed for obtaining pressure distributions about hydrodynamic bodies.

DESCRIPTION OF EQUIPMENT AND CIRCUIT

Considerable care is necessary in designing and constructing an electrolytic tank. The walls and bottom should be plane, and opposite walls should be parallel to each other and perpendicular to the bottom and to adjacent walls. Provision should be made for leveling the tank to make the bottom horizontal, levels for this purpose can be seen on the sides of the steel frame in Figure 1. The conducting plates which constitute the electrodes should be plane and aligned parallel to each other and perpendicular to the bottom and adjacent walls. It is equally important that the rails and cross beams for supporting the probe carriage be carefully aligned with the tank walls so that the probe may be moved in true longitudinal and transverse directions without canting.

The electrolytic tank which was designed and built at the Taylor Model Basin consists of a steel tank with a lining of insulating material; see Figure 1. The inside dimensions are 46 × 27 7/8 in. on the bottom and may be filled to a depth of 15 in. Two pairs of heavy copper electrodes are available, one pair for the long sides of the tank and another pair for the short sides. The probe for exploring the electric field may be supported either on the arm of a

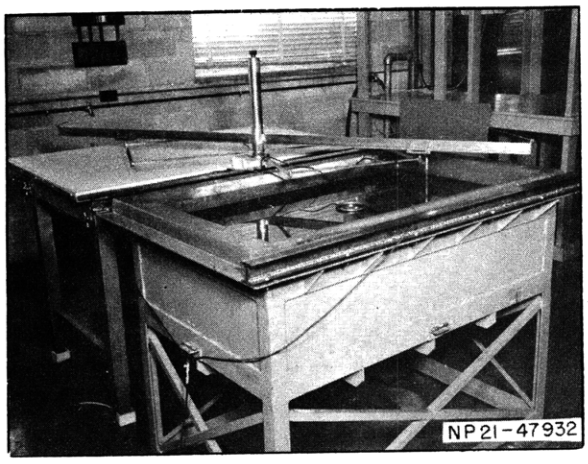

Figure 1a - Electrolytic Tank Fitted with Pantograph

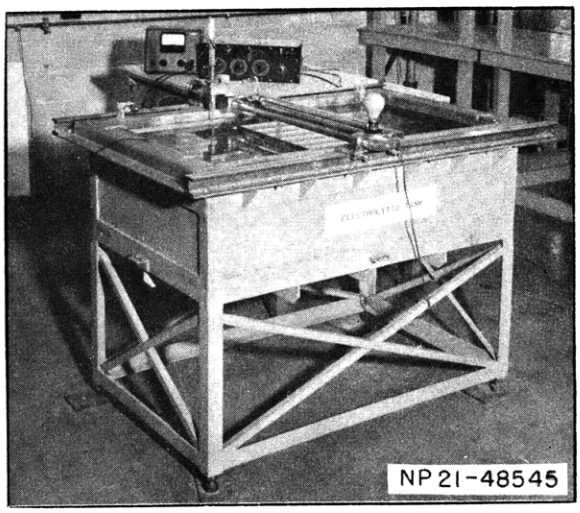

Figure 1b - Electrolytic Tank Fitted with Cross Beams and Carriage

Figure 1 - General Views of the Electrolytic Tank

pantograph or on a small carriage mounted on cross beams which slide on a pair of rails fastened to the long sides of the tank.

The tank lining adopted for the TMB electrolytic tank was cast of a wax compound (30 percent aristo and 70 percent beeswax), and the surfaces were made smooth and plane by hand scraping. This type of lining was adopted after considerable trouble was encountered with a glass lining. The glass plates were difficult to seal and they cracked easily. It was important to avoid leaks as it was impossible to operate with a low resistance between the electrolyte and the metal frame. The presence of beeswax in the wax compound makes the lining more pliable and less apt to crack with changes in temperature. Moreover, cracks in the wax are easily repaired.

The velocity and pressure distributions about two-dimensional bodies are investigated in the TMB tank with the use of Analogy A by placing dielectric cylindrical bodies at the center of the tank or by mounting half of the cylinder on one of the vertical tank walls. Similarly, in the study of three-dimensional bodies of revolution, a quarter body is mounted on one of the vertical walls and the water level is brought exactly to the axis of the body. In both cases, the electric field is explored by probing the surface of the electrolyte in contact with the body.*

The dielectric models used with Analogy A have been machined out of the same hard wax compound that is used for ship models at the Taylor Model Basin,[9] and they are sprayed with Krylon, a waterproofing plastic compound which is hydrophobic, to eliminate the meniscus

*It is hoped that a technique can be developed for determining the pressure distribution about three-dimensional bodies with only one or two planes of symmetry, such as a ship model. The field about such bodies will be explored beneath the surface with a slender insulated probe with only the tip exposed.

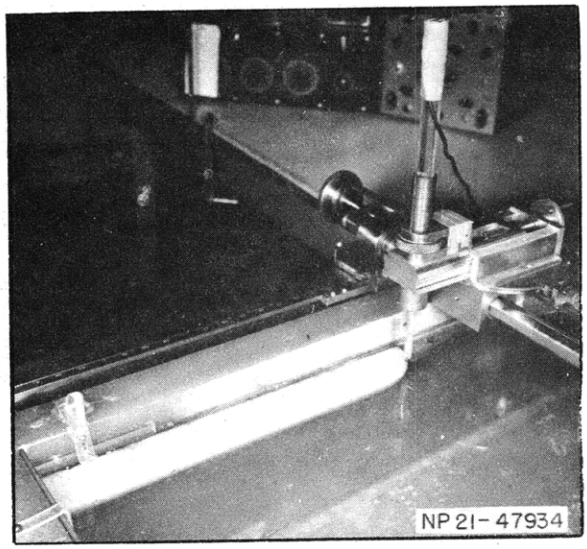

Figure 2a - Probing Along the Contour of a Wax Model of a Half Body

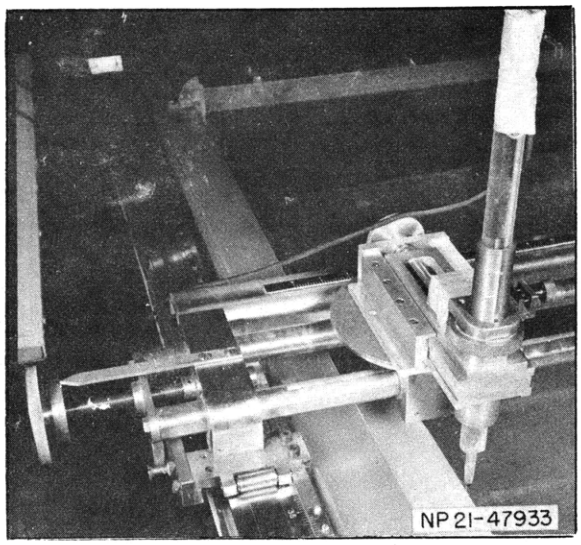

Figure 2b - Probe Mount Showing the Micrometer Screws for x, y, and z Motions

Figure 2 - Views of the Probe Mounted on the Cross Beams

at the water surface. Since it is difficult to hold tolerances of a few thousands of an inch with wax models it will be necessary to machine future models out of plastic material.

The pantograph shown in Figure 1a is useful for plotting lines of constant electrical potential in the vicinity of a body. In two-dimensional flow, streamlines are easily obtained as lines of constant electrical potential if the body is a conductor and Analogy B is used. Points may be located within $\pm$ 0.01 in. with the pantograph.

If the velocity and pressure distributions about a body are required, greater precision may be obtained by using the probe mounted on a carriage (Figures 1b and 2). The carriage is supported by cross beams which move longitudinally on rails parallel to the sides of the tank. Longitudinal and transverse motions may be adjusted by micrometer screws. The height of the probe may be varied by means of a coarse screw with a calibrated head. Hence, displacements in all three directions may easily be determined within 0.001 in. or better.

Two methods were investigated for finding pressure distributions, the double-probe method first described by Taylor and Sharman[3] and the single-probe method. Analogy A is used in both methods and the potentials or potential differences are obtained with potentiometer circuits and a null instrument. The single probe is used for probing in contact with the body, and the double probe is used for obtaining the pressure field away from the model.

The circuit used in exploring the pressure distribution with a single probe is shown in Figure 3. A pair of copper electrodes is set up parallel to each other at opposite ends of the tank and is fed with 110-volt alternating current. Tap water was found to be a satisfactory electrolyte. The potential at the probe is obtained by adjusting the capacitance C and the voltage divider R for a null reading of the null instrument. The ratio of the potential at the probe to the potential across the tank is read from the voltage divider.

The construction of the voltage divider R is shown in Figure 4. The resistors in each bank are noninductive precision resistors, accurate within $\pm$ 0.25 percent. A slide wire potentiometer is used in the last stage for fine adjustment. Thus the potential at the probe may be read to six figures, with an uncertainty in the fifth or sixth place depending upon the stability of the rest of the circuit. Although an accuracy of four significant figures in the potential may be sufficient for obtaining a pressure distribution about a large model with gradual changes in curvature, it is necessary to obtain five and sometimes six significant figures in the potential about small bodies where the curvature changes rapidly.

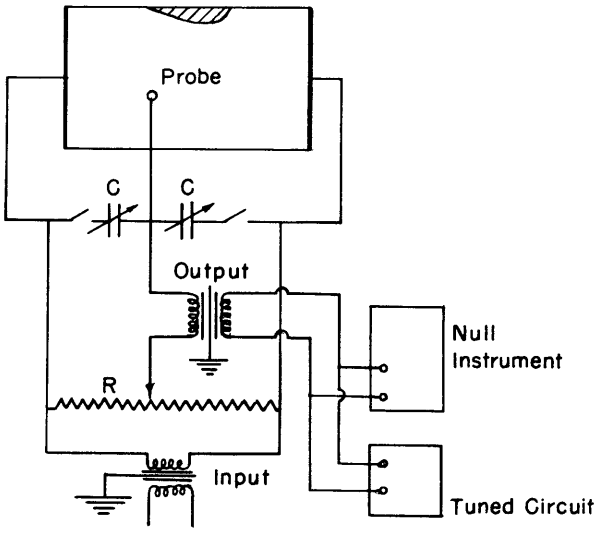

Figure 3 - Wiring Diagram of the Electric Circuit Used with the Single Probe

The sensitivity and stability of the electrical circuit are improved by eliminating electrical pickup and ground loops, by avoiding polarization of the electrolyte at the probe and electrodes, and by eliminating phase shifts in the circuit to the null instrument.

To eliminate ground loops and extraneous pickup, isolation transformers are inserted in the input and output circuits and the leads from the probe are shielded. The insertion of a tuned circuit across the leads to the null instrument excludes extraneous frequencies and greatly improves the sensitivity of the null reading.

Polarization of the electrolyte about the probe and the electrodes manifests itself as an instability in the null reading. In those experiments where four-place accuracy in the potential is sufficient, polarization was not particularly troublesome even when a 60-cycle power supply was used. If greater precision is needed in the potential readings, precautions have to be taken to eliminate polarization. Polarization may be reduced by increasing the frequency of the power supply and by coating the probe and electrodes with Aquadag. With the Aquadag coatings, the null reading could be stabilized to give five significant figures in the potential reading with a 400-cycle input and was further improved with a 1000-cycle power input. Polarization was found to be less troublesome with the tank full of water than with a depth of only a few inches.

Little is gained in obtaining great precision in the potential reading unless the position of the probe can be determined with like precision. For this reason, micrometer adjustments for positioning the probe were installed. In probing in contact with a model, it is extremely important to bring the probe into contact with the model without bending the tip. An error of a few hundredths of an inch in the position of the probe may result in an error of several percent in a pressure distribution. To avoid bending the probe, an auxiliary circuit was set up in which

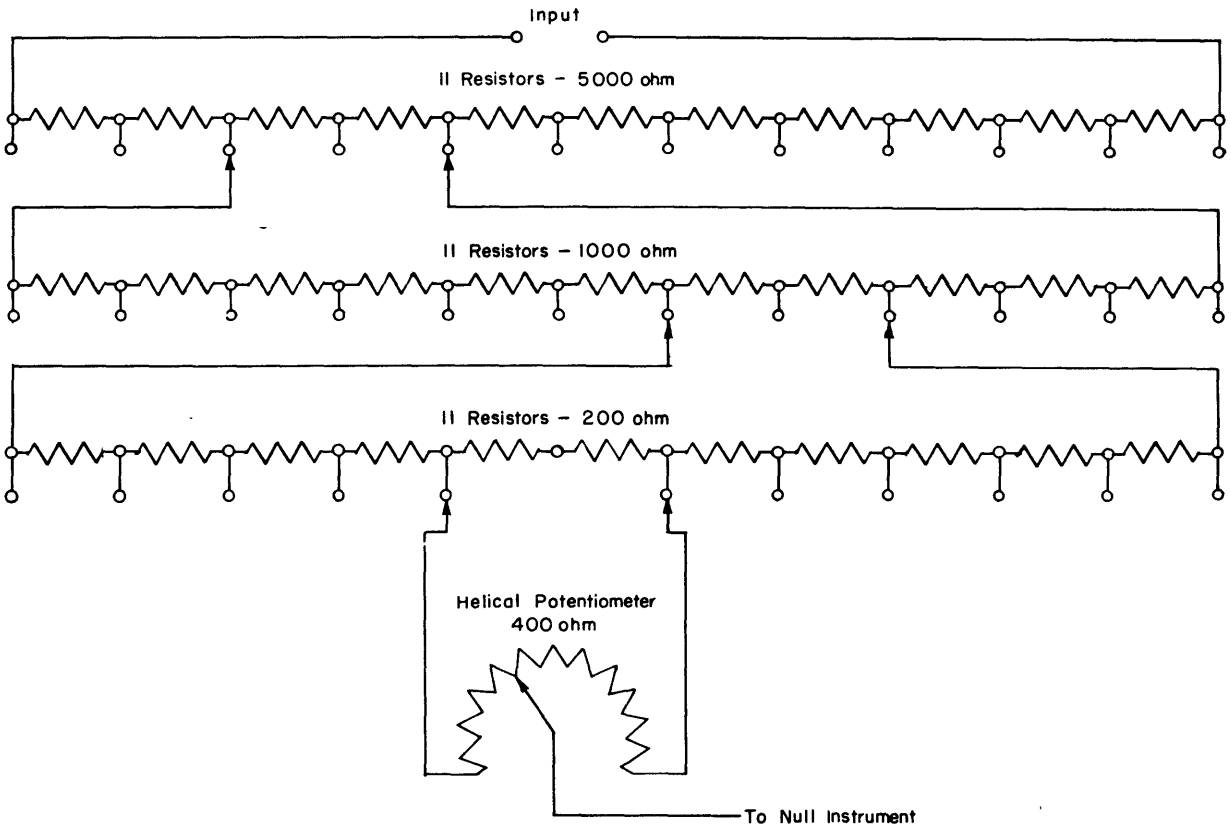

Figure 4 - Diagram of the Decade Voltage Divider

a flashlight bulb would light as soon as contact was made between the probe and the model. For this purpose, a fine wire, a few mils in diameter, is stretched along the contour of the model just above the water surface, and the auxiliary circuit is triggered when the probe just touches the wire. The auxiliary circuit is opened before the potential reading is taken. Careful manipulation of the micrometer screws enables contact with the body to be made without danger of bending the tip.

An electronic voltmeter with a low range of 0.005 volts together with a preamplifier was used as a null instrument. This instrument proved to be more sensitive than a cathode-ray oscillograph in obtaining a null reading. As it was impossible to eliminate all pickup from the circuit, it was difficult to obtain an undistorted Lissajous figure with the high amplification needed.

Although the double probe is not useful for probing in contact with a model, it is very useful for exploring the velocity and pressure fields away from the model. In probing in contact with the model, it would not be possible to use the technique of a fine wire along the contour and there would be danger of bending the tips and changing the spacing between them. However, the double-probe method has several important advantages in exploring the field away from the body. It is more convenient since potential differences, which are proportional to the velocities, are found directly without making a differentiation. For detecting small

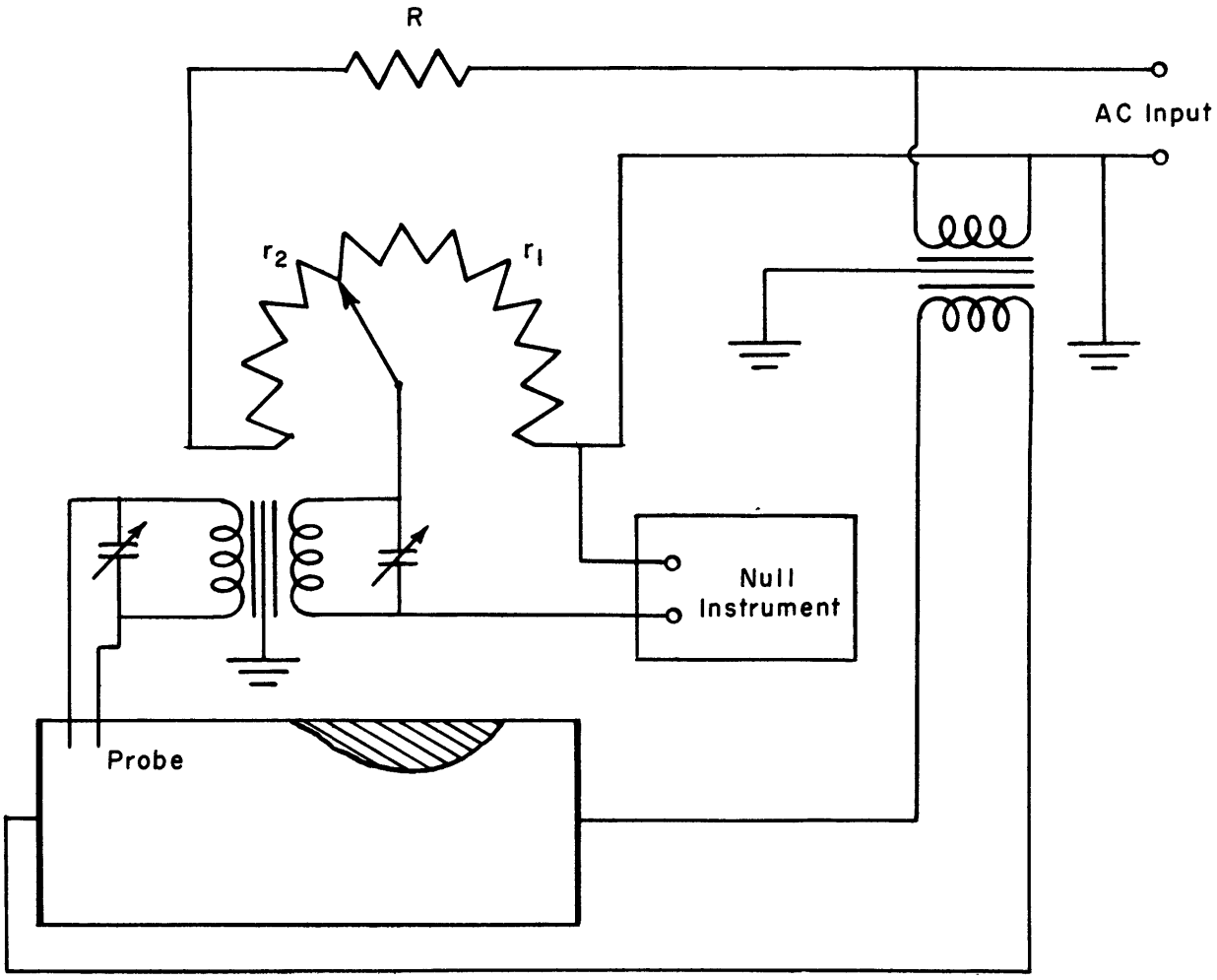

Figure 5 - Wiring Diagram of the Electric Circuit Used with the Double Probe

pressure changes with a single probe, the sensitivity of the circuit must be pushed to its limit where instability arising from polarization becomes troublesome. Polarization appears to be less troublesome with the double-probe circuit, and potential differences can be obtained to three significant figures with an uncertainty of no more than 1 in the third place.

The circuit used with the double probe which was developed at Dr. Malavard's laboratory[7] is shown in Figure 5. The potential across the double probe is balanced by the potential across r_1 which is

$$\frac{\Delta V}{V} = \frac{r_1}{R + r_1 + r_2} \qquad [13]$$

where V is the input potential. The resistances r_1 and r_2 are the resistances on either arm of a slide wire voltage divider of about 100 ohms, and R is of the order of 100,000 ohms. The exact value of R depends upon the voltage gain or loss in the probe circuit and upon the desired range of r_1. Then

$$\frac{u}{U_0} = \frac{r_1}{r_{1_0}} \qquad [14]$$

where r_{1_0} corresponds to the free-stream velocity U_0 taken at a point far from the model.

A transformer with a high input impedance was chosen for the probe circuit, in order to avoid drawing current from the tank and changing the potential between the probes. An input voltage of either 400 or 60 cycles may be used as this circuit appears to be less sensitive to polarization than the single-probe circuit. The insertion of capacitors of suitable size across the primary or secondary of the transformer in the probe circuit eliminates phase shifts in the circuit and makes it possible to obtain a sharper null reading.*

Since the voltage to the tank electrodes is supplied through an isolation transformer, it is necessary to connect the plates and auxiliary circuit in such a manner that the potentials oppose each other. Furthermore, since the circuit consists of two independent subcircuits, a small change in input voltage will change the over-all sensitivity of the circuit. For this reason, it is necessary to use a well-regulated voltage supply. In all studies with the double-probe technique at the Taylor Model Basin, the greatest source of error has been in the instability of the input voltage which introduces an uncertainty in the value of the free-stream velocity.

PROCEDURE FOR FINDING PRESSURE DISTRIBUTIONS BY THE SINGLE-PROBE METHOD

Analogy A, in which a dielectric body is mounted in the tank, is used for finding pressure distributions. The electrodes are positioned on the transverse walls so that the equivalent flow is in the longitudinal or x direction. Before the body is mounted in the tank, the equivalent free-stream velocity U_0 is determined from the gradient of the potential along the length of the tank. The curve obtained by plotting the electric potential V against x should be linear if the tank is properly leveled and the plates properly aligned.

The model is mounted in the tank and carefully aligned with the longitudinal rail. The potential field about the body is determined in such a manner that the potential gradient along the contour of the model may be determined. When the arc length of the body as a function of x is known, the potential may be determined for small increments in x without regard for the value of y at different stations along the body. Then the potential gradient along the contour is

$$\frac{dV}{ds} = \frac{dV}{dx}\frac{dx}{ds} \qquad [15]$$

*The double-probe circuit has recently been improved by inserting a Wagner ground across the probe circuit and eliminating the capacitors.

When the arc length as a function of x is not known, the increments in s must be computed from the measured increments of x and y.

$$\Delta s = \left[\Delta x^2 + \Delta y^2 \right]^{1/2} \qquad [16]$$

With the micrometer screw adjustment, Δs may be determined to better than one thousandth of an inch.

When $\frac{dV}{ds}$ has been determined, the ratio of the tangential velocity to the free-stream velocity is given by

$$\frac{v_t}{U_0} = \frac{dV}{ds}\left(\frac{dV}{dx}\right)_0^{-1} \qquad [17]$$

TABLE 1

Comparison of Experimental and Theoretical Data for Velocity and Pressure Distributions on a Sphere

$\frac{x}{r}$	$\frac{s}{r}$	$\frac{v_t}{U_0}$ Experimental	$\frac{v_t}{U_0}$ Theoretical	$1-\left(\frac{v_t}{U_0}\right)^2$ Experimental	$1-\left(\frac{v_t}{U_0}\right)^2$ Theoretical
0.996	0.08	0.128	0.148	0.984	0:978
0.988	0.16	0.214	0.232	0.954	0.946
0.976	0.24	0.337	0.327	0.886	0.893
0.956	0.32	0.464	0,440	0.785	0.806
0.926	0.40	0.577	0.566	0.667	0.677
0.892	0.48	0.694	0.678	0.518	0.540
0.852	0.56	0.805	0.785	0.352	0.373
0.804	0.64	0.902	0.892	0.186	0.204
0.752	0.72	0.972	0.989	0.055	0.022
0.696	0.80	1.061	1.077	-0.126	-0.160
0.636	0.88	1.160	1.158	-0.346	-0.340
0.572	0.96	1.233	1.230	-0.520	-0.514
0.508	1.04	1.307	1.292	-0.708	-0.669
0.436	1.12	1.349	1.350	-0.820	-0.822
0.376	1.20	1.391	1.390	-0.935	-0.932
0.284	1.28	1.436	1.438	-1.062	-1.068
0.204	1.36	1.452	1.469	-1.108	-1.157
0.128	1.44	1.481	1.488	-1.193	-1.213
0.048	1.52	1.504	1.498	-1.262	-1.245
0.008	1.56	1.504	1.500	-1.262	-1.250

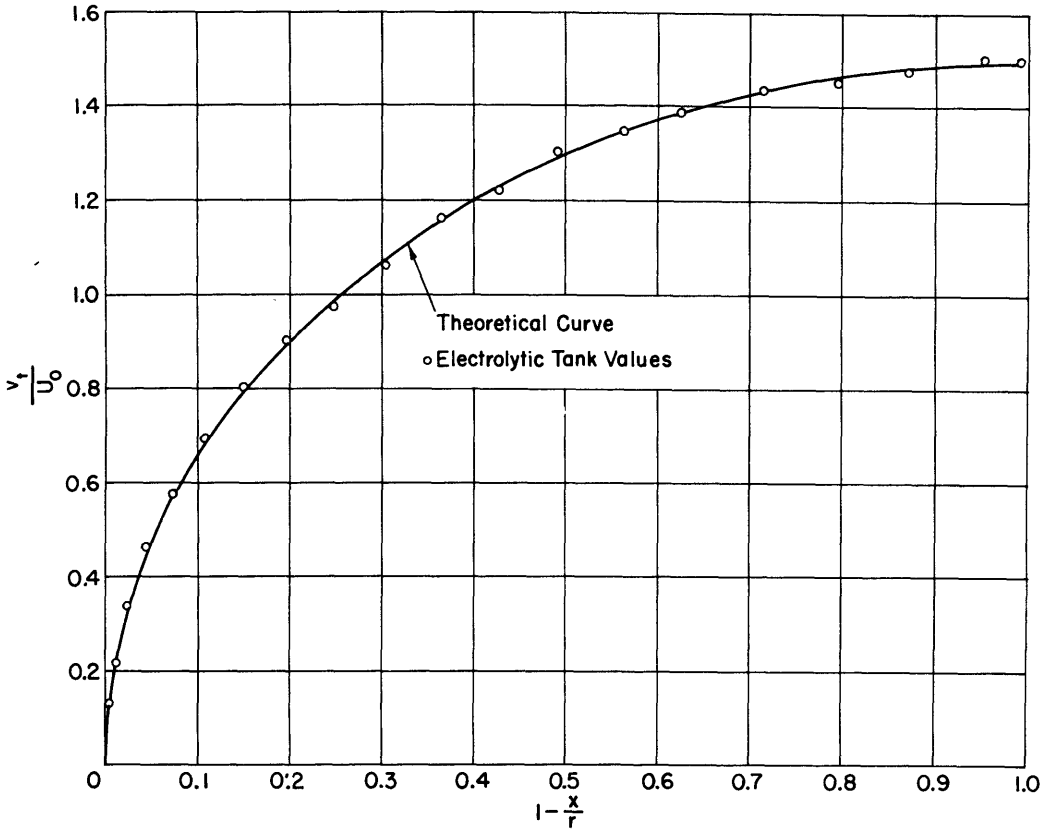

Figure 6 - Velocity Distribution About a Sphere

where $\left(\frac{dV}{dx}\right)_0$ is the potential gradient in the tank without the model.

The pressure coefficient at each point is found by the equation

$$\frac{p}{\frac{1}{2}\rho U_0^2} = 1 - \left(\frac{v_t}{U_0}\right)^2 \qquad [18]$$

In the following examples, the experimental techniques used vary slightly for the different bodies as improvements were made in the apparatus, instrumentation, and methods of analysis.

SPHERE

The first body of revolution investigated in the TMB electrolytic tank was a sphere. The model was a quarter section of a wax sphere 2.5 in. in radius; it was mounted on a polystyrene plate which was aligned along one of the longitudinal walls of the tank. This body was studied before the introduction of the fine wire on the section above the water surface or the installation of the micrometer screws for the x and y motions; 60-cycle alternating current was used without a tuned circuit across the null instrument. Under these conditions, the

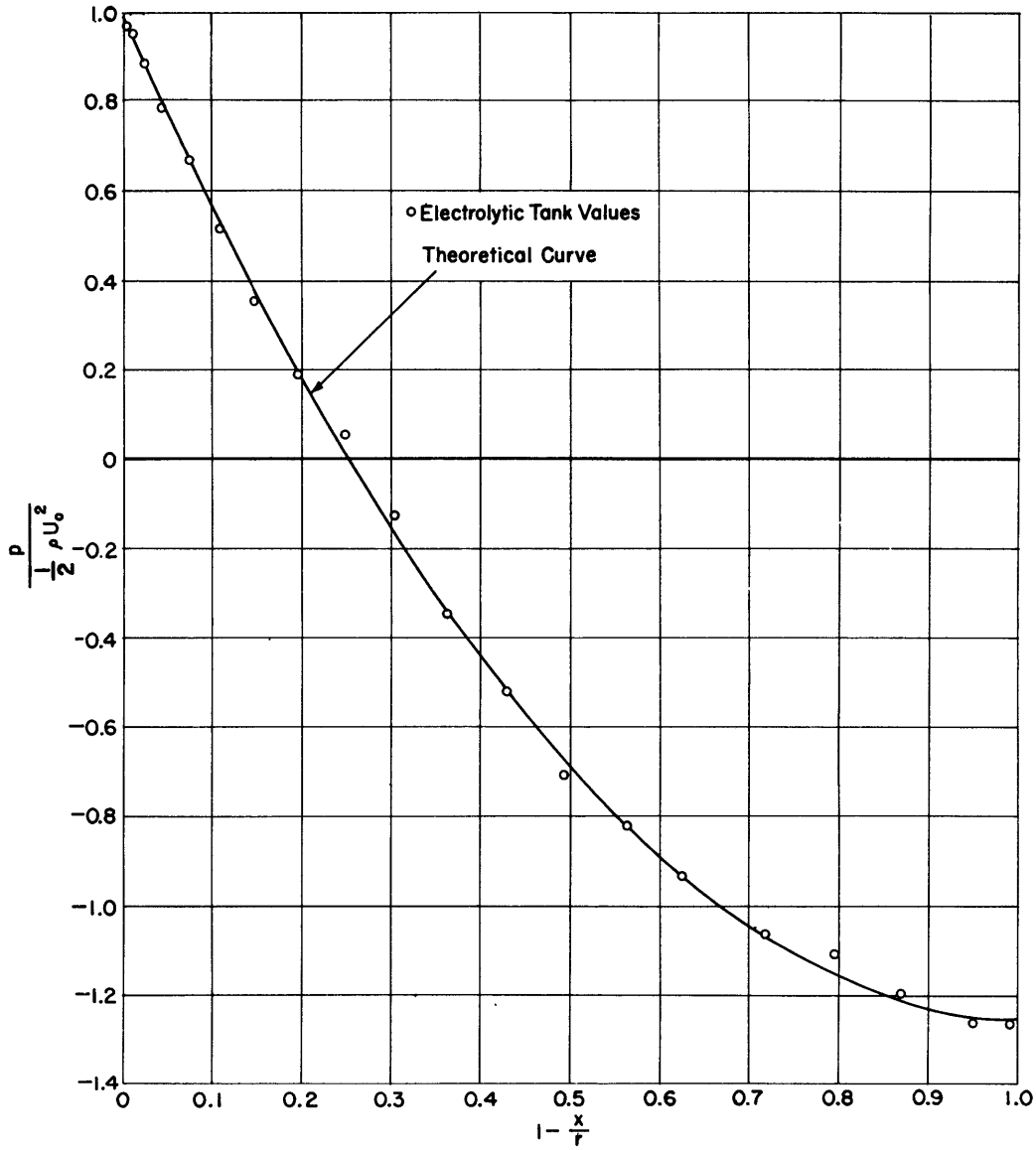

Figure 7 - Pressure Distribution About a Sphere

potential could be read to five significant figures, with some uncertainty in the last place. The potential was determined all along the contour in increments of 0.01 in. in the x direction. Since the arc length s as a function of x is known for a sphere, V was plotted directly as a function of s on a scale large enough to include all the significant figures of the measurements, and a faired curve was drawn through the points. The slopes at representative points were computed by the extrapolation method described in Appendix A, using points from a faired curve through the experimental points. The tangential velocity coefficients obtained from these slopes using Equation [17] and the pressure coefficients obtained from Equation [18] are recorded in Table 1 together with the theoretical values. Graphs of the velocity and pressure coefficients are shown in Figures 6 and 7.

ELONGATED BODY OF REVOLUTION

A quarter body of an elongated body of revolution was mounted on the side wall of the tank in the same manner as the sphere. The body chosen was one for which the velocity and pressure distribution had been determined by the theoretical method developed by Landweber.[10] The equation of the body is

$$y^2 = 0.04(1 - x^4) \qquad [19]$$

The model was made of wax with a length of 20 in. and a midsection radius of 2 in. The micrometer screws for x and y motions of the carriage had been added to the tank when this model was studied, but other improvements had not been made.

TABLE 2

Reduced Data for the Elongated Body of Revolution

x	$\frac{dx}{ds}$	$\frac{1}{U_0}\frac{dV}{dx}$	$\frac{v_t}{U_0}$	$\frac{p}{\frac{1}{2}\rho U_0^2}$
0.00	1.000	1.018	1.018	−0.036
0.05	1.000	1.018	1.018	−0.036
0.10	1.000	1.019	1.019	−0.038
0.15	1.000	1.024	1.024	−0.049
0.20	1.000	1.030	1.030	−0.061
0.25	1.000	1.036	1.036	−0.073
0.30	0.999	1.043	1.043	−0.088
0.35	0.999	1.051	1.051	−0.105
0.40	0.999	1.059	1.059	−0.121
0.45	0.999	1.067	1.067	−0.138
0.50	0.998	1.075	1.074	−0.153
0.55	0.997	1.071	1.078	−0.162
0.60	0.996	1.090	1.085	−0.177
0.65	0.993	1.099	1.090	−0.188
0.70	0.988	1.108	1.094	−0.197
0.75	0.980	1.117	1.093	−0.195
0.80	0.966	1.125	1.088	−0.184
0.82	0.958	1.128	1.082	−0.171
0.84	0.948	1.131	1.076	−0.158
0.86	0.935	1.134	1.062	−0.128
0.88	0.918	1.140	1.046	−0.094
0.90	0.895	1.142	1.022	−0.044
0.92	0.863	1.144	0.987	+0.026
0.94	0.796	1.150	0.915	+0.163
0.96	0.739	1.153	0.851	+0.276
0.98	0.594	1.157	0.687	+0.528

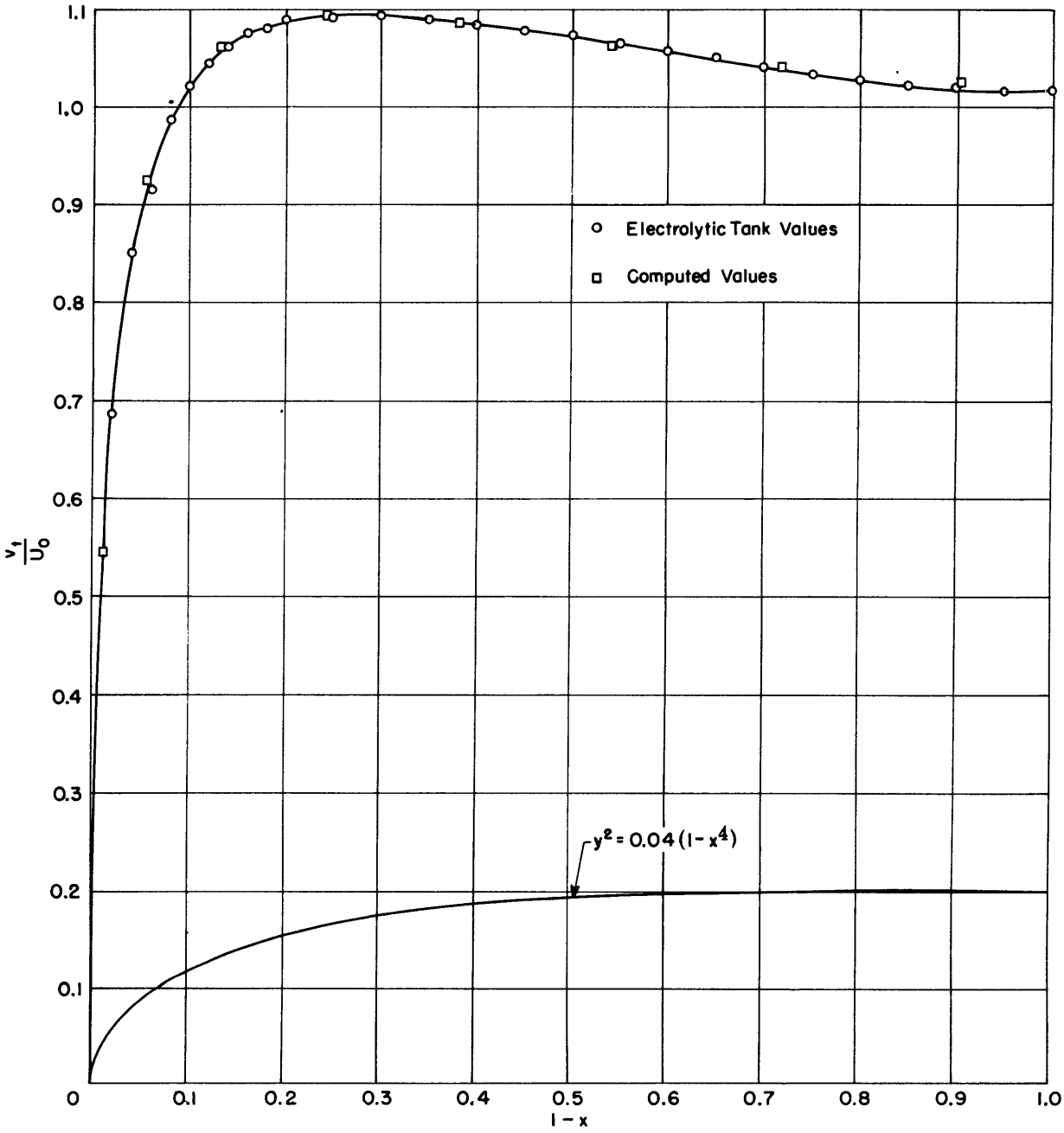

Figure 8 - Velocity Distribution About an Elongated Body of Revolution

The potential was determined at 0.2-in. intervals over the flat section of the body and at finer intervals near the nose where the curvature is greater. The potential V was plotted as a function of x since $\frac{ds}{dx}$ was known from Landweber's analysis. The x component of the potential gradient was found from the faired curve through the experimental points as described in Appendix A. The tangential velocities were obtained from Equation [17]. The experimental values of the velocity and pressure distributions are tabulated in Table 2 and are plotted in Figures 8 and 9. The values computed by Landweber's theoretical method are

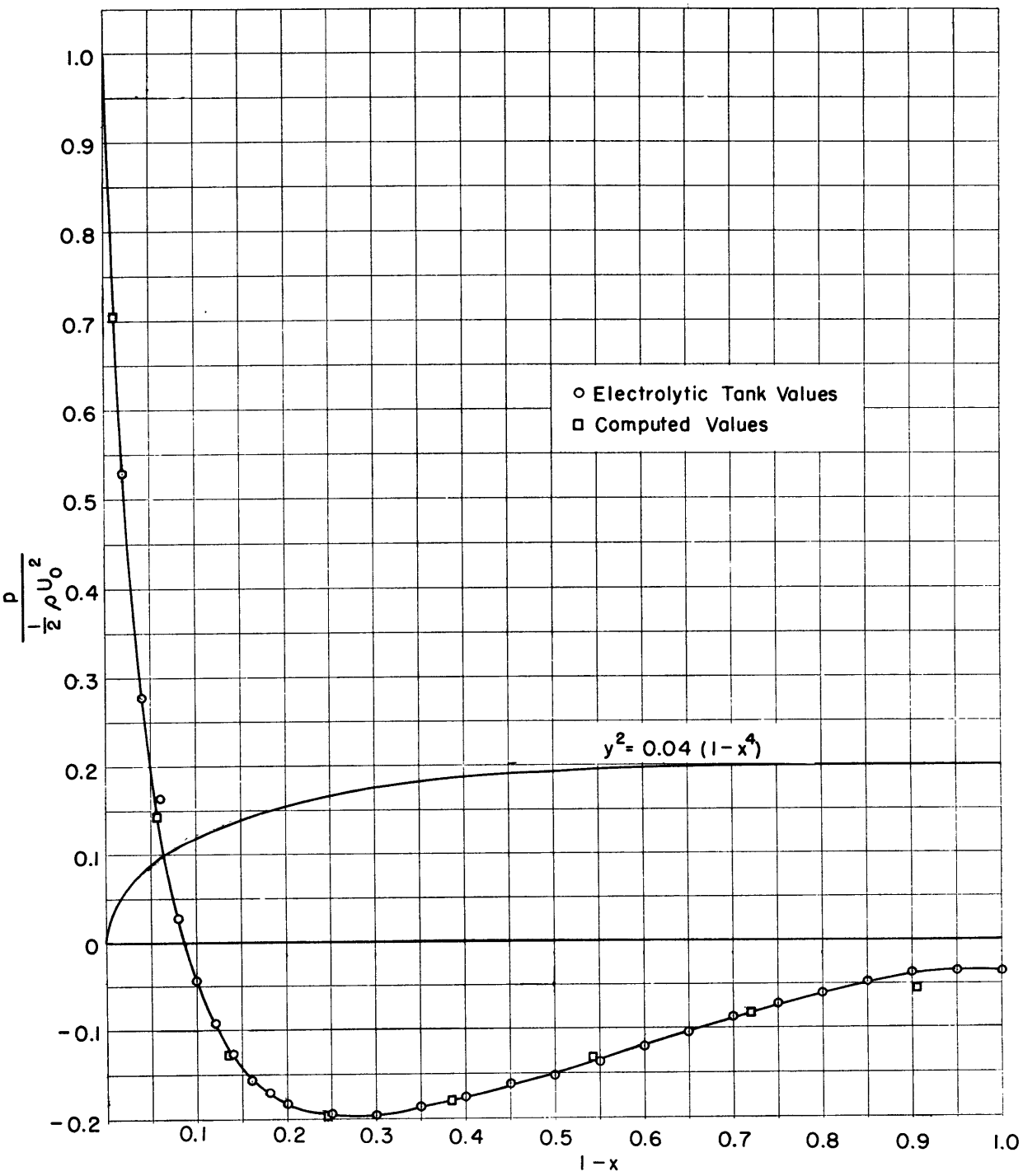

Figure 9 - Pressure Distribution About an Elongated Body of Revolution

shown in Figures 8 and 9 and are tabulated in Table 3.

The points obtained from the analysis of the electrolytic tank data are compared with those obtained by a theoretical analysis by Landweber's method in Figure 9. It is seen that discrepancies are small everywhere except for a section near the middle of the body. A check of the body offsets show a mound 0.04 in. high and 3 in. broad about 3/4 in. beyond the center

TABLE 3

Values of the Velocity and Pressure Coefficients for the Elongated Body of Revolution Computed by Landweber's Method

x	y	$\frac{v_t}{U_0}$	$\frac{p}{\frac{1}{2}\rho U_0^2}$
0.9894	0.0409	0.5450	0.7030
0.9446	0.0903	0.9261	0.1423
0.8656	0.1324	1.0619	-0.1276
0.7554	0.1643	1.0946	-0.1981
0.6179	0.1848	1.0864	-0.1803
0.4580	0.1956	1.0641	-0.1323
0.2816	0.1994	1.0416	-0.0849
0.0950	0.2000	1.0276	-0.0560

of the body. Hence, the pressure obtained between stations 0.8 and 1.0 on the body appear low due to the retardation of the stream in approaching the mound. Although the theory given in Appendix B does not give a good approximation for the flow approaching a mound, the increase in velocity over the mound would produce a decrease in pressure coefficient of about 0.03. The increase in pressure obtained just ahead of the mound is of this order of magnitude.

TORPEDO MODEL H-60

A quarter body of torpedo model H-60 was machined out of wax and mounted on the side wall in one corner of the tank; see Figure 2a. In order to simulate a body infinitely long, the model was made 18 in. in length (which was as long as practicable) and was cemented to one of the electrodes to increase its effective length. The parallel section of the model had a radius of 2 in.

The probing about the nose of this body for obtaining the potential gradients required greater precision than for the other bodies because of the large curvature and the rapidly changing potential gradient over this region. It was while working with this body that the wire along the contour just above the waterline was introduced and that the 400-cycle alternating current was substituted for the 60-cycle. These refinements became necessary because the potential differences as well as the increments in arc length were small. Potential readings were made at from 0.02- to 0.03-in. intervals over short segments at different stations along the body. Increments in arc length were obtained from Equation [16] from the measured increments in x and y. With the use of the fine wire along the body contour, there was no difficulty in reading the x and y coordinates in thousandths of an inch, and readings would

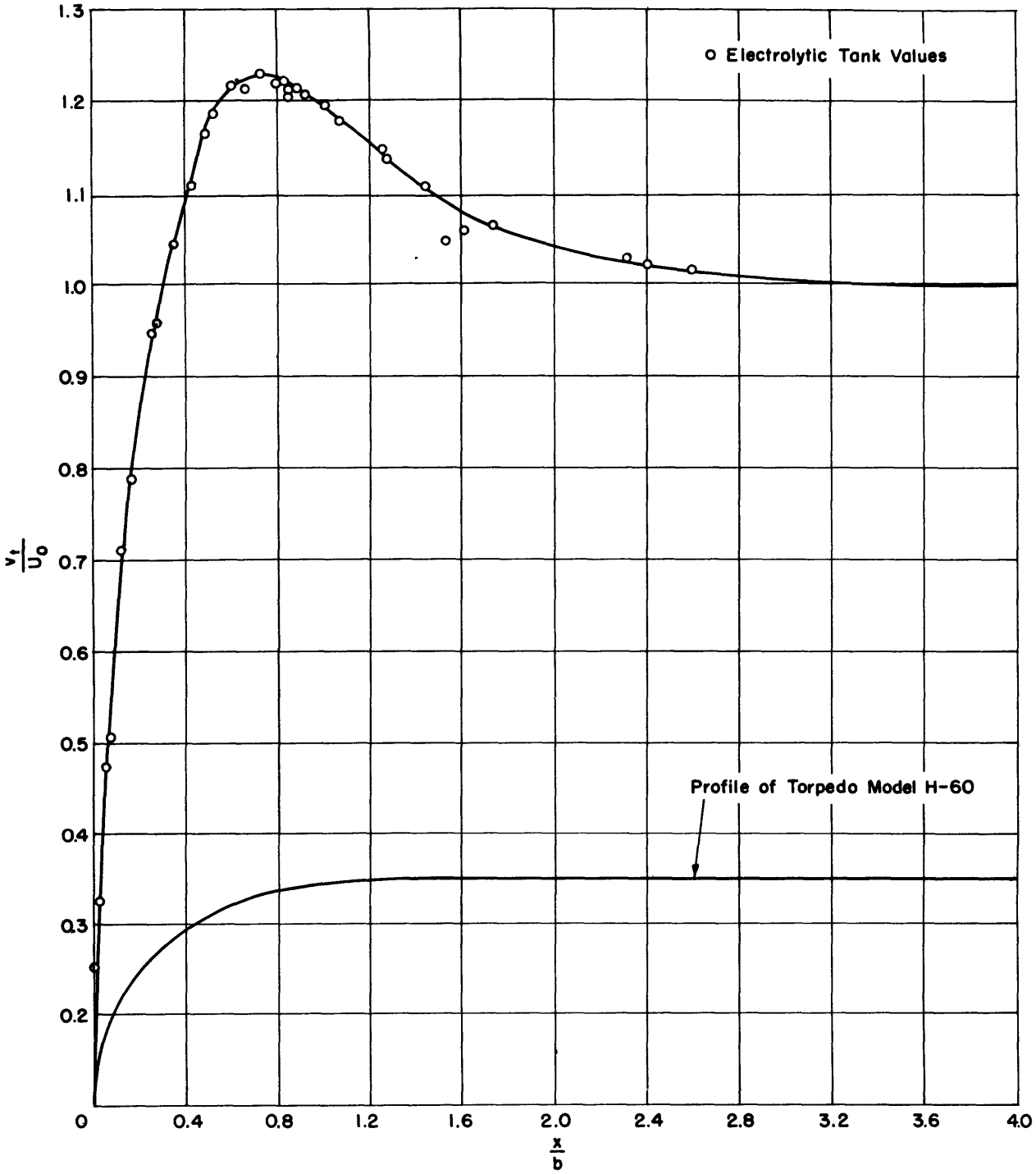

Figure 10 - Velocity Distribution About Torpedo Model H-60

repeat well. With the 400-cycle voltage input and the 400-cycle tuned circuit across the null instrument, the potential could be read to six significant figures, with an uncertainty of from 3 to 5 in the last place. The extrapolation method described in Appendix A was used in computing the potential gradients, but there was no need to use values of V and s from a faired curve since they had been measured to a sufficient number of significant figures.

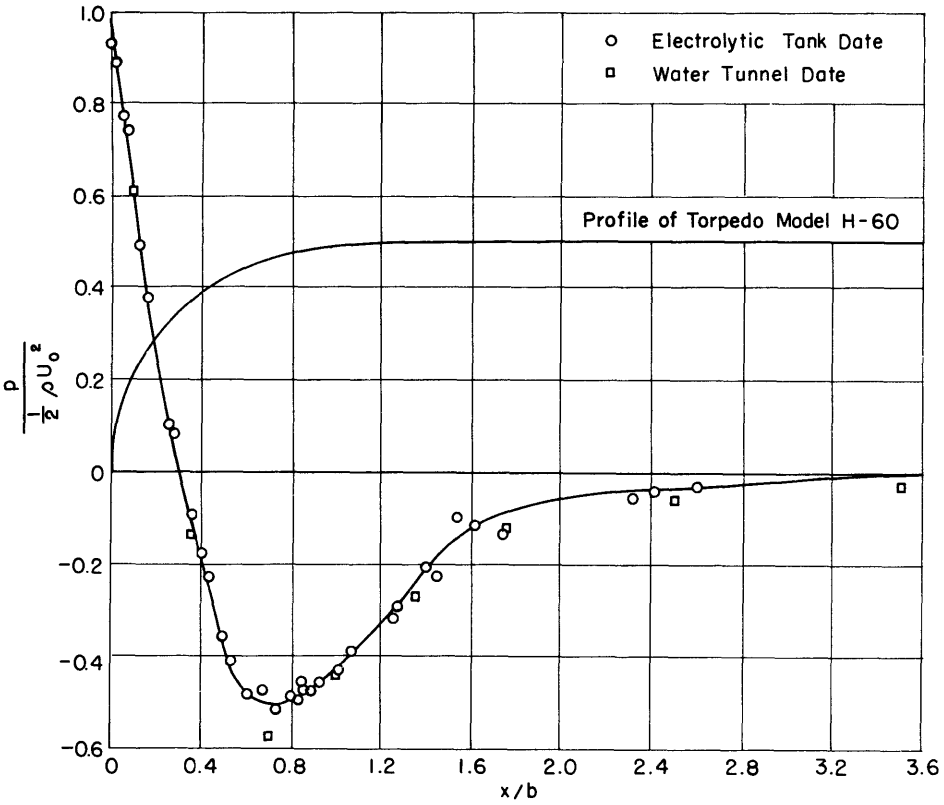

Figure 11 - Pressure Distribution About Torpedo Model H-60

The velocity and pressure distributions obtained about model H-60 are shown in Figures 10 and 11 and tabulated in Table 4. The experimental pressure measurements made with piezometer openings in a model tested in the water tunnel are also shown in Figure 11. It is seen that the pressures obtained in the electrolytic tank are consistently higher than those obtained in the water tunnel. This discrepancy is believed to be caused by errors in machining the model. The curve of Figure 12 is drawn from the actual offsets of the wax electrolytic tank model while the correct offsets are indicated by circles. The two sets of offsets are drawn to be coincident at the nose. It is seen that the offsets from the electrolytic tank model do not fair into the straight section as fast as they should. If the forward part of the body may be represented by a prolate spheriod, the error increases the effective semimajor axis and the eccentricity.

The method of computing the error in pressure coefficient from changes in eccentricity of a prolate ellipsoid is described in Appendix B. If the method is applied to compute the change in semimajor axis necessary to give the observed change in minimum pressure coefficient, the semimajor axis would have to increase about 10 percent. As this is the right order of magnitude for the increase in the semimajor axis, the observed pressure distribution appears to be consistent.

The irregularity in the pressure distribution for x/b between 1.4 and 1.7 may be accounted for by a small surface irregularity in this region.

TABLE 4

Experimental Data for Velocity and Pressure Distributions for Torpedo Model H-60

$\frac{x}{b}$	$\frac{v_t}{U_0}$	$\frac{p}{\frac{1}{2}\rho U_0^2}$
0.003	0.252	0.936
0.026	0.324	0.895
0.056	0.474	0.775
0.074	0.507	0.743
0.122	0.711	0.494
0.163	0.789	0.378
0.257	0.947	0.103
0.281	0.958	0.083
0.358	1.044	−0.090
0.403	1.084	−0.174
0.435	1.108	−0.227
0.495	1.165	−0.356
0.530	1.187	−0.408
0.607	1.217	−0.480
0.665	1.213	−0.472
0.735	1.230	−0.513
0.800	1.219	−0.486
0.835	1.222	−0.492
0.850	1.205	−0.453
0.855	1.213	−0.471
0.888	1.214	−0.474
0.925	1.207	−0.456
0.012	1.195	−0.428
1.070	1.178	−0.388
1.255	1.148	−0.317
1.275	1.136	−0.291
1.400	1.097	−0.203
1.445	1.106	−0.223
1.535	1.046	−0.095
1.615	1.058	−0.112
1.740	1.064	−0.131
2.320	1.028	−0.056
2.410	1.021	−0.041
2.600	1.015	−0.031

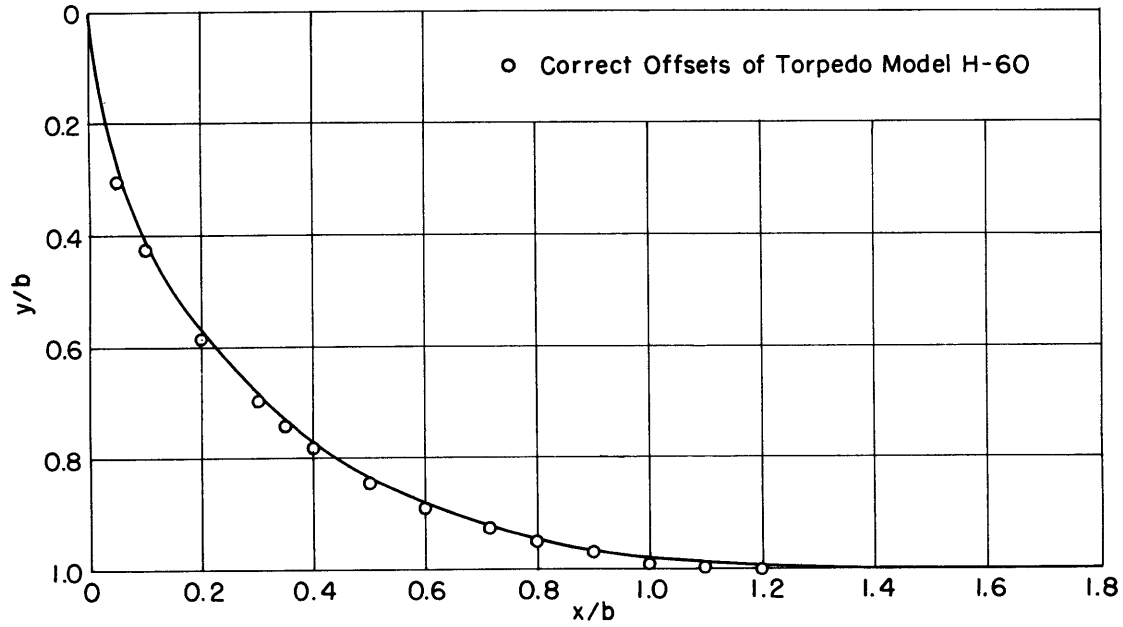

Figure 12 - Comparison of the Offsets of the Wax Electrolytic-Tank Model of H-60 with the Correct Offsets

PROCEDURE FOR FINDING PRESSURE FIELDS BY THE DOUBLE-PROBE METHOD

To demonstrate the usefulness and reliability of the double-probe method in obtaining the field of pressure in the vicinity of a body, the field about the 2.5 in. radius sphere was mapped. The sphere was mounted on the longitudinal wall as described in the single-probe experiment, and the potential gradients in the x and y directions were obtained along longitudinal lines at various distances from the centerline. The velocity and direction of flow are obtained from the resultant potential gradient, and the pressure coefficient is obtained from Equation [18] where v_i^2 is now the square of the resultant velocity.

A reference point was found in the tank far enough from the model that free-stream conditions could be assumed to hold. The equivalent free-stream velocity was checked quite frequently to ensure that the line voltage had not changed and altered the sensitivity of the circuit. As the 400-cycle generator was not available for this investigation, it was necessary to use the 60-cycle line voltage with a voltage regulator. In spite of the voltage regulator, surges in line voltage often changed the potential gradient at the reference point by as much as 1 percent.

The data were obtained at convenient intervals at constant distances out from the longitudinal wall of the tank. In order to fix the relative positions of the curves, potential gradients were obtained along transverse lines at several representative stations. In this way, errors arising from drifts in sensitivity of the circuit could be recognized and corrected.

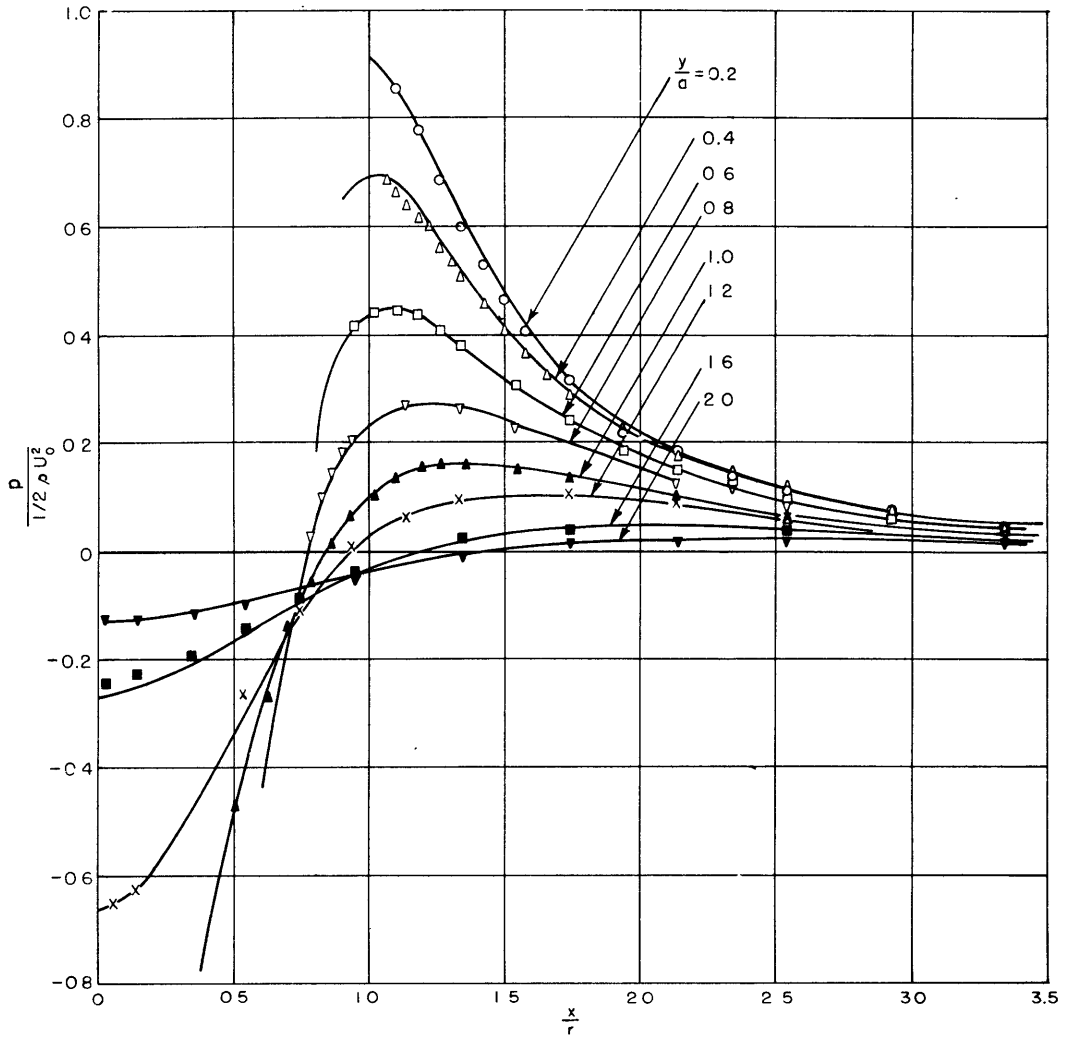

Figure 13 - Pressure Field in a Meridian Plane About a Sphere

(Solid lines are theoretical curves.)

The pressure field obtained in a meridian plane about the sphere is shown in Figure 13; the solid curves show the corresponding theoretical values. The scatter of the points from the theoretical curves is equivalent to an error of about 1 percent in determining the velocity. As the potential gradient can usually be obtained within 1 part in 500, the rest of the error is in the free-stream value or in setting the probe.

PERSONNEL

The electrolytic tank project was initiated by P. Eisenberg who prepared the preliminary design. The development of the tank, its equipment, and the experimental procedures were carried out by A. Borden with the assistance of W.E. Ball, Jr., and G.L. Shelton, Jr. The report was checked by P. Granville.

APPENDIX A

GRAPHICAL EXTRAPOLATION METHOD FOR DETERMINING THE SLOPE OF A CURVE

Any short segment of a curve which is continuous and fair may be approximated by a quadratic equation of the form

$$y = ax^2 + bx + c \qquad [20].$$

To obtain the slope of the curve, the differential quotient $\Delta y/\Delta x$ is found. At a neighboring point $x + \Delta x$, $y + \Delta y$ the approximate equation of the curve is

$$y + \Delta y = a(x + \Delta x)^2 + b(x + \Delta x) + c \qquad [21].$$

The slope of the curve between these two points is

$$\frac{\Delta y}{\Delta x} = 2ax + b + a\Delta x \qquad [22].$$

Since $2ax + b$ is constant for any selected point, the slope is a linear function of Δx.

To determine the slope at a point x_0, y_0, the x and y coordinates of four or five points on one side of this point are recorded at convenient small intervals. Then the following differential quotients are obtained

$$\frac{\Delta y_1}{\Delta x_1} = \frac{y_1 - y_0}{x_1 - x_0}, \quad \frac{\Delta y_2}{\Delta x_2} = \frac{y_2 - y_0}{x_2 - x_0} \qquad [23]$$

If the values of these quotients are plotted against Δx on a large scale, the faired curve through them should be a straight line which, when extrapolated to $\Delta x = 0$, gives the slope at the point x_0, y_0. If the faired curve is not a straight line, the last increments chosen are too large to satisfy the approximation made in Equation [21]. In practice it is preferable to obtain the differential quotients on both sides of the selected point and use the best line through all the points to find the intercept. This process makes it possible to obtain an extra significant figure in the slope of the curve.

APPENDIX B

EFFECT OF ERRORS IN BODY SHAPE ON RESULTING VELOCITY AND PRESSURE DISTRIBUTIONS

Errors in body shape may arise from misalignment of the body in the tank or from errors in machining. If the model may be approximated by a prolate ellipsoid, the errors in machining may produce a change in the eccentricity of the equivalent ellipsoid. On the other hand, a small mound or depression on a section where the transverse curvature is small may be treated as two-dimensional flow over a mound or depression. The error in pressure distribution produced by changes in eccentricity has been reported by Eisenberg,[11] and the flow past a mound or depression is treated in standard texts on hydrodynamics, such as that by Milne-Thompson.[12] The results of these investigations will be outlined here.

The pressure coefficient for a prolate spheriod at an angle of attack α can be shown to be[11]

$$\frac{p}{\frac{1}{2}\rho U_0^2} = 1 - \left\{ \eta^2 \left(\frac{1-\mu^2}{1-e^2\mu^2} \right) \cos^2 \alpha + \frac{\mu \eta \beta}{1-e^2\mu^2} \sqrt{(1-e^2)(1-\mu^2)}\, \sin 2\alpha \cos \omega \right. \tag{24}$$

$$\left. + \beta^2 \left[1 - \left(\frac{1-\mu^2}{1-e^2\mu^2} \right) \cos^2 \omega \right] \sin^2 \alpha \right\}$$

where

$$\eta = e^2 \left[1 - \frac{1-e^2}{2e} \ln \frac{1+e}{1-e} \right]^{-1} \tag{25}$$

$$\beta = 2e^2 \left[1 - 2e^2 - \frac{1-e^2}{2e} \ln \frac{1+e}{1-e} \right]^{-1} \tag{26}$$

The eccentricity

$$e = \sqrt{1 - \frac{b^2}{a^2}} \tag{27}$$

where a and b are the semimajor and semiminor axes of the ellipsoid. Also, μ equals $\frac{x}{a}$ where x is measured from the minor axis, and ω is the angle between a meridian plane and the xy plane. At zero angle of attack, the minimum pressure coefficient at $\mu = 0$ is

$$\left(\frac{p}{\frac{1}{2}\rho U_0^2}\right)_{min} = 1 - \eta^2 \qquad [28]$$

The change in minimum pressure coefficient for a small change in eccentricity is

$$\Delta\left(\frac{p}{\frac{1}{2}\rho U_0^2}\right)_{min} = \frac{2\eta^2(2\eta + e^2 - 3)}{(1 - e^2)} \frac{\Delta e}{e} \qquad [29]$$

where Δe, obtained from differentiating Equation [27], is given approximately by

$$\Delta e = \frac{1 - e^2}{e}\left(\frac{\delta a}{a} - \frac{\delta b}{b}\right) \qquad [30]$$

Although the shape of the body may depart appreciably from the shape of an ellipsoid, the required value of the eccentricity for the above equations may be found for that ellipsoid which has the same minimum pressure coefficient as the body investigated. Then the errors in the semimajor and semiminor axes of the body may be used to estimate the change in eccentricity.

To find the effect of a slight misalignment of the body, Equation [24] may be differentiated with respect to α. The change in pressure coefficient for small angles of attack ($\alpha = 0$) is[11]

$$\Delta\left(\frac{p}{\frac{1}{2}\rho U_0^2}\right) = -\frac{2\mu\eta\beta}{1 - e^2\mu^2}\sqrt{(1 - \mu^2)(1 - e^2)}\,\Delta\alpha \qquad [31]$$

The greatest change of pressure occurs not at the pressure minimum, $\mu = 0$, but at

$$\mu_\alpha = \pm\left[2 - e^2\right]^{-1/2} \qquad [32]$$

At this point

$$\left(\frac{p}{\frac{1}{2}\rho U_0^2}\right)_\alpha = 1 - \frac{1}{2}\eta^2 \qquad [33]$$

and

$$\Delta\left(\frac{p}{\frac{1}{2}\rho U_0^2}\right)_\alpha = -\beta\eta\,\Delta\alpha \qquad [34]$$

This analysis shows that although a small change in α may not affect the pressure minimum appreciably, it may produce changes in the shape of the pressure distribution curve.

The error introduced by a small mound or depression in a body may be approximated by the two-dimensional flow over the arc of a circle extending from $+c$ to $-c$ on the x axis. The complex potential for this flow is given by[12]

$$w = \frac{2ciU_0}{n} \cot \frac{\xi + i\eta}{n} \qquad [35]$$

where

$$z = x + iy = ic \cot \frac{\xi + i\eta}{2} \qquad [36]$$

The stagnation streamline is obtained by letting $\xi = \frac{1}{2} n\pi$ over the arc of the circle and $\xi = 0$ on the plane. The shape of arc is determined by the parameter n, with $n = 2$ representing flow over a flat plate, $n > 2$ representing flow over a depression, and $n < 2$ representing flow over a mound.

The curves η = constant are another set of circles othogonal to the first set and with centers on the x axis. At the center of the arc $x = 0$, $\eta = 0$, and at the edges $x = \pm c$, $\eta = \pm \infty$.

For small mounds or depressions where the height t is small compared with the half width c

$$\xi = \frac{n\pi}{2} = \pi \pm \frac{t}{c} \qquad [37]$$

Equation [37] may be used to determine n.

The complex velocity over the arc of a circle may be found by differentiating Equation [35] with respect to z

$$v_x - iv_y = -\frac{4U_0}{n^2} \left(\frac{\sin \frac{\xi + i\eta}{2}}{\sin \frac{\xi + i\eta}{n}} \right)^2 \qquad [38]$$

The square of the resultant velocity is then

$$\frac{v_x^2 + v_y^2}{U_0^2} = \frac{16}{n^4} \left(\frac{\cosh \eta - \cos \xi}{\cosh \frac{2\eta}{n} - \cos \frac{2\xi}{n}} \right)^2 \qquad [39]$$

Equation [37] may be used to eliminate ξ and n. For small values of t/c near the center of the arc

$$\frac{v_x^2 + v_y^2}{U_0^2} = \left(1 \pm 4\,\frac{t}{\pi c}\right)\left(\frac{1 + \cosh \eta}{1 + \cosh \eta \pm \frac{t\eta}{\pi c} \sinh \eta}\right)^2 \qquad [40]$$

The plus signs are used for a mound and the minus signs for a depression. At the center of the arc where $\eta = 0$, the squared expression reduces to unity. Toward $x = \pm c$, the velocity approaches zero for a mound and infinity for a depression. Since such abrupt changes in slope would not be likely to be encountered on a machined body, Equation [40] should be used only for points near the center of the arc where η is small.

REFERENCES

1. Enclosure (A) to TMB CONFIDENTIAL ltr C-S75-1 to BuOrd dated 9 May 1947.

2. Relf, E.F., "An Electrical Method for Tracing Streamlines Around Bodies in a Perfect Fluid," Aeronautical Research Committee, Reports and Memoranda No. 905, 1924.

3. Taylor, G.I. and Sharman, C.F., "A Mechanical Method for Solving Problems of Flow in Compressible Fluids," Aeronautical Research Committee, Reports and Memoranda No. 1195, 1928.

4. Malavard, L., "Application des Analogies Électriques à la Solution de Quelques Problemes de l'Hydrodynamique," Publications Scientifiques et Techniques du Ministère de l'Air No. 57, 1934.

5. Malavard, L., "Étude de Quelques Problèmes Techniques Relevant de la Théorie des Ailes," Publications Scientifique et Techniques du Ministère de l'Air, No. 153, 1939.

6. Malavard, L., "The Use of Rheo-Electric Analogies in Certain Aerodynamical Problems," Journal of Royal Aeronautical Society, Vol. 51, No. 441, pp. 739, September 1947.

7. Surugue, J., "Technique Générales du Laboratoire de Physique," Vol II, Chapter 15, (L. Malavard, "La Techniques des Analogies Electriques"), Edition du CNRS, Paris, 1950.

8. Lamb, H., "Hydrodynamics," American Reprint Edition, University Press, Cambridge, England, 1945.

9. Couch, Richard B., "The Development of Wax Ship Model Manufacturing at the Taylor Model Basin," TMB Report 728, August 1950.

10. Landweber, L., "The Axially Symmetric Potential Flow About Elongated Bodies of Revolution," TMB Report 761, August 1951.

11. Eisenberg, P., "Effect of Small Errors in Body Shape and Angle on Pressure Distribution and Cavitation Limits," TMB Report 792, October 1951.

12. Milne-Thompson, L.M., "Theoretical Hydrodynamics," The MacMillan Co., New York, 1950, p. 167.

INITIAL DISTRIBUTION

Copies	
19	Chief, Bureau of Ships, Technical Library (Code 327), for distribution: 5 Technical Library 1 Deputy and Assistant to Chief (Code 101) 1 Technical Assistant to Chief (Code 106) 3 Research (Code 300) 2 Applied Science (Code 370) 2 Preliminary Design (Code 420) 1 Submarines (Code 515) 2 Minesweeping (Code 520) 1 Torpedo Countermeasures (Code 520I) 1 Sonar (Code 845)
9	Chief, Bureau of Ordnance 5 Underwater Ordnance 1 for Dr. A. Miller 2 Mines 2 Aerodynamics and Hydrodynamics Branch
5	Chief of Naval Research 3 Fluid Mechanics 1 Undersea Warfare 1 Armaments
3	Chief, Bureau of Aeronautics, Aerodynamics and Hydrodynamics Branch
2	Commander, U.S. Naval Ordnance Laboratory, White Oak, Silver Spring 19, Md.
3	Commander, U.S. Naval Ordnance Test Station, Inyokern, China Lake, Calif. 2 copies for Pasadena Annex
1	Commander, Mare Island Naval Shipyard, Vallejo, California
1	Commander, Portsmouth Naval Shipyard, Portsmouth, N. H.
1	Commander, New York Naval Shipyard, Brooklyn 1, N. Y.
1	Commander, Norfolk Naval Shipyard, Portsmouth, Va.
1	Commanding Officer and Director, U.S. Navy Underwater Sound Laboratory, Fort Trumbull, New London, Conn.
1	Commanding Officer and Director, U.S. Navy Electronics Laboratory, San Diego 52, Calif.
1	Commanding Officer, U.S. Naval Underwater Ordnance Station, Newport, R.I.
1	Commanding Officer, U.S. Navy Mine Countermeasures Station, Panama City, Fla.
2	Director, U.S. Naval Research Laboratory, Washington 25, D.C.
1	Director, U.S. Waterways Experiment Station, Vicksburg, Miss.
1	Superintendent, U.S. Naval Postgraduate School, Monterey, Calif.

Copies

Copies	
6	Director of Aeronautical Research, National Advisory Committee for Aeronautics, 1724 F Street, N.W., Washington, D.C.
1	Director, Langley Aeronautical Laboratory, Langley Air Force Base, Va.
1	Director, Woods Hole Oceanographic Institution, Woods Hole, Mass.
1	Director, Technical Information Branch, Aberdeen Proving Grounds, Md.
2	Chairman, Research and Development Board, Department of Defense Building, Washington 25, D. C.
1	Editor, Bibliography of Technical Reports, Office of Technical Services, U. S. Department of Commerce, Washington 25, D. C.
2	Newport News Shipbuilding and Dry Dock Company, Newport News, Va. 1 copy for Senior Naval Architect 1 copy for Supervisor, Hydraulics Laboratory
2	Director, Experimental Towing Tank, Stevens Institute of Technology, 711 Hudson Street, Hoboken, N. J.
3	Director, Iowa Institute of Hydraulic Research, State University of Iowa, Iowa City, Iowa 1 copy for Dr. Phillip G. Hubbard
3	Director, Ordnance Research Laboratory, Pennsylvania State College, State College, Pa. 1 copy for Dr. J. M. Robertson
2	Hydrodynamic Laboratory, California Institute of Technology, Pasadena 4, Calif. Attn: Executive Committee
2	Bureau of Aeronautics Representative, Cornell Aeronautical Laboratory, Cornell Research Foundation, Box 235, Buffalo 21, N. Y. 1 copy for Dr. D. H. Garber
2	Director, St. Anthony Falls Hydraulic Laboratory, University of Minnesota, Minneapolis 14, Minn.
2	Director, Experimental Naval Tank, Department of Naval Architecture and Marine Engineering, University of Michigan, Ann Arbor, Mich.
1	Director, Applied Physics Laboratory, Johns Hopkins University, 8621 Georgia Ave., Silver Spring, Md.
2	Director, Institute for Fluid Dynamics and Applied Mathematics, University of Maryland, College Park, Md. 1 copy for Dr. Weinsten
1	Director, Institute of Aeronautical Sciences, 2 East 64th Street, New York 21, N.Y.
2	Aerojet Engineering Corporation, Underwater Engine Division, Azusa, Calif. 1 copy for Mr. S. Krumbholz
1	Administrator, Webb Institute of Naval Architecture, Crescent Beach Road, Glen Cove, Long Island, N. Y.

Copies

1 Chairman, Department of Aeronautical Engineering, New York University, University Heights, New York 53, N. Y.

1 Chairman, Department of Engineering Mechanics, University of Michigan, Ann Arbor, Mich.

2 Head, Department of Naval Architecture and Marine Engineering, Massachusetts Institute of Technology, Cambridge 39, Mass.

1 Head, Department of Civil Engineering, Colorado A and M College, Fort Collins, Colo.

1 Librarian, Daniel Guggenheim Aeronautical Laboratory, California Institute of Technology, Pasadena 4, Calif.

1 Librarian, Pacific Aeronautical Library, Institute of Aeronautical Sciences, 7660 Beverly Blvd., Los Angeles 36, Calif.

2 Dr. V.L. Streeter, Illinois Institute of Technology, 300 Federal Street, Chicago 16, Ill.

1 Dr. C. C. Lin, Department of Mathematics, Massachusetts Institute of Technology, Cambridge 39, Mass.

1 Prof. W. S. Hamilton,Technical Institute, Northwestern University, Evanston, Ill.

1 Prof. Garrett Birkhoff, Harvard University, Cambridge, Mass.

1 Prof. K. E. Schoenherr, School of Engineering, University of Notre Dame, Notre Dame, Ind.

1 Dr. A. G. Strandhagen, School of Engineering, University of Notre Dame, Notre Dame, Ind.

1 Dr. D. Gilbarg, Department of Mathematics, University of Indiana, Bloomingdale, Ind.

1 Prof. J. Vennard, Department of Civil Engineering, Stanford University, Calif.

1 Dr. G. F. Wislicenus, Mechanical Engineering Department, Johns Hopkins University, Baltimore 18, Md.

1 Prof. R. G. Folsom, Department of Engineering, University of California, Berkeley 4, Calif.

1 Prof. J. L. Hooper, Alden Hydraulic Laboratory, Worcester Polytechnical Institute, Worcester, Mass.

1 Dr. M. S. Plesset, California Institute of Technology, Pasadena 4, Calif.

1 Dr. V. L. Schiff, Stanford University, California

1 Mr. C. A. Lee, Hydraulic Engineer, Research and Development Laboratories, Kimberly-Clark Corporation, Neenah, Wis.

Copies

1	Dr. C. Kaplan, Langley Aeronautical Laboratory, Langley Air Force Base, Va.
1	Dr. H. Reissner, Brooklyn Polytechnic Institute, Brooklyn, N. Y.
1	Dr. L. Mayerhoff, Brooklyn Polytechnic Institute, Brooklyn, N.Y.
1	Dr. J. V. Wehausen, Editor, Mathematical Reviews, American Mathematical Society, 80 Waterman Street, Providence 6, R. I.
1	Mr. John A. Cole, Lubrication Project, Engineering Laboratory, Harvard University, 50 Oxford Street, Cambridge 38, Mass.
1	Mr. William B. Brower, Jr., Department of Aeronautical Engineering, Rensselaer Polytechnic Institute, Troy, N. Y.
2	Editor, Applied Mechanics Reviews, Midwest Research Institute, 4049 Pennsylvania, Kansas City 2, Mo.
1	Editor, Aeronautical Engineering Review, 2 East 64th St., New York, N. Y.
9	British Joint Services Mission, (Navy Staff), P.O. Box 165, Benjamin Franklin Station, Washington, D. C.
1	Dr. F. Ursell, Trinity College, Cambridge, England
1	Dr. G. K. Batchelor, Cambridge University, Cambridge, England
1	Head, Aerodynamics Division, National Physical Laboratory, Teddington, Middlesex, England
1	Dr. R. Timman, National Luchtvaartlabortorium, Stoterwag 145, Amsterdam, The Netherlands
1	Head, Aeronautics Department, Imperial College, London SW 7, England
1	Principal, College of Aeronautics, Cranfield, Bletchley, Bucks, England
1	Head, Engineering Department, Nottingham University, Nottingham, England
1	Director, British Shipbuilding Research Association 5, Chesterfield Gardens, Curzon Street, London W.1, England
1	Editor, Physics Abstracts, Institution of Electrical Engineers, Savoy Place, London, W.C.2, England
1	Editor, Index Aeronautics, Ministry of Supply, Milbank, London S.W. 1, England
3	Director, Hydrodynamics Laboratory, National Research Council, Ottawa, Canada
1	Prof. Georg Weinblum, Ingenieurschule Z620, Berliner Tor 21, Hamburg, Germany
1	Prof. J. K. Lunde, Skipsmodelltanken Tyholt Trondheim, Norway
1	Superintendent, Netherlands Ship Model Basin, Haagsteeg 2, Wageningen, The Netherlands
1	Prof. J. M. Burgers, Laboratorium Voor Aero- En Hydrodynamica, Nieuwe Laan 76, Delft, The Netherlands

Copies

1	Director, Swedish State Shipbuilding Experimental Tank, Göteborg 24, Sweden
1	Director, Aeronautical Research Institute of Sweden, Ranhammarsvagen 12, Ulsvunda, Sweden
1	Directeur du Bassin d'Essais Des Carénes, 6, Boulevard Victor, Paris XV, France
2	Dr. L. Malavard, Office National d'Études et de Recherches Aéronautiques, Chatillon, Paris, France
1	Directeur, Laboratoire Dauphinois d'Hydraulique des Ateliers, Neyrpic, Avenue de Beauvert, Grenoble, (Isére), France
1	Office National d'Études et de Recherches Aéronautiques 3, rue Léon Bonnat, Paris XVI, France
1	Prof. J. Ackeret, Institute für Aerodynamik Der Eidgenössiche, Zürich, Switzerland
1	Dr. Jun-ichi Okabe, The Research Institute for Applied Mechanics, Kyushu University, Hakozaki-machi, Fukuoki-shi, Japan
1	Dr. Ir. J. Balhan, Technische Hogeschool, Sub-Afdeling der Scheepsbouwkunde, Nieuwe Laan 76, Delft, The Netherlands
1	Gen. Ing. U. Pugliese, Presidente Instituto Nazionale per Studi ed Esperienze di Architettura Navale via della Vasca Navale 89, Rome, Italy
1	Sr. M. Acevedo y Campoamor, Director, Canal de Experienceas Hidrodinamicas, El Pardo, Madrid, Spain
1	Dr. J. Dieudonné, Directeur, Institut de Recherches de la Construction Navale, 1 Boulevard Haussmann, Paris (9e), France
1	Prof. H. Nordstrom, Director, Statens Skeppsprovningsanstalt, Göteborg 24, Sweden
9	U.S. Naval Attaché, Naval Attaché for Air, London, England
3	Canadian Joint Staff, 1746 Massachusetts Ave., N.W., Washington, D.C.

IPPO PRNC WASH D C